Effects of Flame Structure and Flame Strain on the Growth Region of Carbon Nanotubes in Counter-Flow Diffusion Flame

Open Access

Eik Woei Heng[1], Muhammad Thalhah Zainal[1], Mohd Fairus Mohd Yasin[1,*], Norikhwan Hamzah[1]

[1] High Speed Reacting Flow Laboratory (HIREF), School of Mechanical Engineering, Faculty of Engineering, Universiti Teknologi Malaysia, 81310 Skudai, Johor, Malaysia

ARTICLE INFO	ABSTRACT
	The improvement of the carbon nanotube (CNT) synthesis control in flames requires the understanding of the effects of flame structure towards the catalytic growth. A preliminary prediction of growth region in different flame configuration is useful to efficiently improve the synthesis process. A growth rate model based on nickel catalyst that is coupled with a flame model based on computational fluid dynamics (CFD) is employed to predict the synthesized CNT length at different regions within the methane-ethylene diffusion flame with counter-flow configuration. At particle scale, the previously developed particle-scale model was successfully validated against a CNT length measurement in carbon vapour deposition (CVD) experiment. At flame scale, a satisfactory agreement was achieved between the predicted and the measured temperature along the flame centreline. The multi-scale model successfully predicts the growth region of CNT on the rich side of the reaction zone where the temperature range of 1200 K to 1500 K with methane mass fraction of 0.05 (nominal) provides a suitable growth environment for the CNT. Compared to the experimental observation, the predicted region of high growth is accurate within 1 mm. Despite the increase in temperature and carbon precursor concentration in opposing directions of the growth region, the growth rate reduces. The main finding is that the increase in flame strain rate results in a flat growth region which is favourable for efficient scaled-up production. The flat growth region results from the dominance of the inertial effects over the buoyancy effects on the reacting flow field. At high strain rate, the width of high temperature region within the shear layer reduces and the growth region is shifted towards the fuel side in response to the shift in the high temperature location towards the same direction. Interestingly, the parabolic trend of CNT growth rate within the counter diffusion flame is dictated by the temperature distribution while the spatial distribution of high yield region is determined by the flame structure.

1. Introduction

Carbon nanotube (CNT) has drawn attention from researchers worldwide due to its excellent electrical, thermal, and mechanical properties. After over two decades, CNT has become an important material especially in large volume consumer applications such as in composites [1],

---

* *Corresponding author.*
E-mail address: mohdfairus@mail.fkm.utm.my (Mohd Fairus Mohd Yasin)

electronics [2], and energy applications [3]. Hence, reliable and economical production of CNTs is vital to sustain the demand for CNTs. Currently, most of the world supply of CNTs has been produced using catalytic chemical vapour deposition (CCVD) which has been time tested to be a reliable method in large-scale production [4]. However, the application of external heating mechanism, combined with the relatively slow synthesis process has driven up the manufacturing cost using CCVD [4]. Flame synthesis is a promising candidate to replace CCVD in mass production CNT manufacturing due to its efficient and rapid synthesis process [5,6]. Both heat and carbon precursors are supplied from the fuel in an auto-thermal environment of the flame [7]. The ease of continuous production makes flame synthesis suitable for industrial production [8]. Establishment of companies that manufacture flame-based CNTs since 2001 further validate the potential for flame synthesis to be a reliable and profitable synthesis process [8,9].

For the past few decades, countless experimental studies have been carried out to find the best combinations of parameters that affect the growth and quality of CNTs in flames [6,10]. In general, the CNT growth control is challenging due to the multiple parameter space that includes gas composition, temperature, pressure, and catalyst [6,11]. The CNT growth in flame poses difficulties in terms of control due to the high temperature gradient that is coupled to the gas dynamics driven by non-linear response of chemical reaction with temperature [6]. The same phenomena are not present in CCVD that makes the CCVD growth control to be simpler compared to that of the flame synthesis. Successful synthesis within flames relies heavily on the proper control of gas-phase species and temperature for CNT growth [6], which cannot be independently modified in flame. Previous studies on flame synthesis have shown that the type of fuel [12,13], fuel to oxidizer ratio [14,15], diluents [16,17], residence time [18], catalyst preparation [19] and flame strain rates [20-22] can have significant effects towards the CNT growth and morphology.

Accurate modelling of flame synthesis is vital in the future development of flame synthesis to reduce the experimental cost. However, due to the large number of inter-related parameters that are involved in flame synthesis, modelling studies for various burner configuration are scarce [23,24]. A coupled simulation has been implemented for CNT growth in CCVD where the temperature and species solutions that are produced by the flame-scale model are used by the particle-scale model to predict the CNT growth rate. Endo *et al.,* [25] provided a coupled model where the predicted distribution of temperature and species in the CVD furnace from CFD simulation are used to determine the reaction rates for CNT deposition on a catalyst substrate. Kuwana and Saito [26] used CFD simulation results of their CVD reactor as inputs for a particle dynamic equation to predict the formation of catalyst nanoparticles.

A growth rate model for flame synthesis is proposed to describe essential CNT growth processes and predicts carbon deposition rate on a catalyst particle during CNT growth [23]. The same model was extended to predict the CNT length and the catalyst deactivation for catalytic growth of CNT [27] and further refinement was proposed to predict CNT length and growth more accurately [28,29]. Other modelling work on CNT synthesis in flames is done by Wen *et al.,* [24] that focuses on the growth of single-walled carbon nanotubes (SWNT) in premixed flame seeded with Fe(CO)5 catalyst particles. The designed three-steps SWNT growth model is then validated through experimental measurement of SWNT growth taken at different locations within the modelled premixed flame. The 1-D flame in counter-flow burner simplifies the CFD modelling and the gas phase analysis [30] for a systematic study on the effects of temperature-species distribution on the synthesis process.

Strain rate effect is one of the factors that influence the growth rate of CNTs in flame synthesis. Counterflow diffusion flame is a stretched planar flame where the stretch effects of such flames are reviewed by Pitz *et al.,* [31]. Flame stretch effects includes stretch rate and curvature effect. From previous studies, strain rate effect was considered in counterflow diffusion flame synthesis of CNTs

[32,33], where the strain rate is the relative area variation rate of a surface moving with the flame. Counterflow diffusion flame is considered as the positively stretched flame, in which the flow field is two-dimensional while the flame structure is one-dimensional [31]. In other words, velocity varies in both radial and axial direction but temperature, density, and species concentration vary only in the axial direction.

Several literatures reported the change in CNTs morphology [32] and growth region due to the competition with the carbon nano-onions (CNOs) and soot formation [34] at varying strain rate. The increase in strain rate results in the increase in the carbon precursor flow rate while reduces the residence time of the precursors on the CNTs growth site [21,34]. The effect of strain rate on CNTs growth was studied by changing the ratio of fuel and oxidiser flow rates [32,33]. Li *et al.,* [32] mentioned that the influence of strain rate of counterflow flame on CNT growth can be either through the carbon sources available in the environment or residence time, depending on which parameter is dominant. For the case of high strain rate, the residence time of carbon source is relatively short, but more carbon sources produced, and vice versa for low strain rate [32,33]. Li *et al.,* [32] found that the CNTs growth is influenced by the available carbon source instead of the residence time, where increased production of straight synthesized CNTs results in higher strain rate. Moreover, the study of Woo *et al.,* [33] showed that more CNTs are produced at relatively higher strain rate. However, such condition results in a flame with more soot particles compared to the flame with low strain rate. Improved quality of flame synthesized CNTs with lower strain rate was reported, due to the stabilised flame behaviour. The amount of carbon sources are fluctuating for high strain rate, which is due to the oscillation of flame as the strain rate moves toward the flame stability limit [31]. Thus, it can be concluded that high strain rate increases the CNT growth but reduce the quality of the CNTs. Subsequently, the optimum strain rate should be further investigated for future mass production of CNTs.

2. Modelling of Flame Synthesis

2.1 Particle-Scale Model

The growth rate model from reference [28] that was modified from the earlier model [27] was utilized to predict CNT length and growth rate based on the flame simulation results. The growth rate model consists of a system of ordinary differential equations (ODE) describing CNT growth processes that include carbon atoms adsorption on the catalyst surface, transport of carbon atoms through the catalyst particle by diffusion, nucleation, and deactivation of the active sites. The main equation that encompasses these growth processes is represented by the ODE in Eq. (1) that solves for the surface density of carbon atoms on a catalyst particle n_1.

$$\frac{dn_1}{dt} = F_{c1} - \frac{n_1}{\tau_{res}} - R_{d,out} - \sigma_x D_s n_1 n_x - (i+1)\sigma_i D_s n_1 n_i - \Phi_{C1}\left(\frac{n_{p1}+n_{p2}}{\alpha_m n_m A_{np}}\right) \tag{1}$$

The first, second, and third terms on the right hand side of Eq. (1) represent the carbon impingement on catalyst particle F_{c1}, carbon desorption away from the particle, and carbon diffusion through the particle $R_{d,out}$ where τ_{res} is the residence time of the impinged carbon atoms on the catalyst particle before desorption takes place. The fourth and fifth term represents the formation of stable and critical clusters respectively where σ_x, D_s, n_x, σ_i, and n_i represent the capture number of carbon atoms flowing into stable nuclei, diffusivity of carbon atoms in nickel, surface density of the stable cluster, capture number of carbon atoms owing into critical nuclei, and surface density of the critical cluster respectively. The final term describes the deactivation of catalyst particle by means of carbonaceous layer and inactive catalyst particles where variables n_{p1} and n_{p2} are the concentration

of carbonaceous layer and inactive catalyst particles respectively. The constants Φ_{c1}, α_m, n_m, and A_{np} represents the carbon flux due to the deposition of pyrolysis products of hydrocarbon species, the number of carbon monolayer, the surface density of the monolayer, and the surface area of the catalyst particle respectively.

$$F_{c1} = F_{b1}p_1 \exp\left(-\frac{E_{a1}}{k_B T}\right) \tag{2}$$

During the catalytic growth, the catalytic decomposition on the catalyst surface causes the feedstock molecules in the gas phase to dissociate into a number of species including solid carbon atoms. The surface chemistry is modelled by the first term F_{c1} that represents the deposition rate of carbon-containing molecules on the catalyst particle due to collision where a simple chemistry is assumed at the surface. Therefore, the impingement term was defined by Eq. (2) where the effects of temperature on CNT growth rate is more aptly described based on the Arrhenius law [28,35]. The variables p_1, E_{a1}, F_{b1}, and k_B are pre-exponential factor, activation energy for the catalytic decomposition of the fuel molecules, flux of the carbon source molecules and Boltzmann's constant respectively. In addition, F_{c1} also captures important CNT growth parameters such as temperature, species partial pressure, and carbon source type. In the present model, F_{c1} is divided with the growth area which is assumed to be constant to ensure unit consistency. The change in the active catalyst surface due to the deactivation effects is not taken into account in this particular term. The system of ODE is numerically solved where the solution of n_1 is used to calculate CNT length and growth rate. The equation for CNT length is shown in Eq. (3) where C^* represents the amount of carbon atoms required for the formation of a carbon monolayer. A detailed description of the ODE system for the growth rate model is included in the other publication [28].

$$L = \left[\frac{1}{a_c C^*}\sqrt{\frac{D_b}{\pi}}\right] \times \int_0^t \frac{n}{\sqrt{t}}dt \tag{3}$$

Since the nature of flame synthesis that involves non-uniform temperature gradient and species distribution, the model implemented input arrays of temperature and species mass fraction from the flame solution with the necessary conversion of the partial pressure to mass fraction. The surface chemistry that describes the effect of catalyst on fuel decomposition is modelled by the impingement term F_{c1}, which describes a simple catalytic decomposition of carbon source molecules to carbon atoms via a single step reaction [28,36]. In the present model, methane that is the most abundant hydrocarbon species in the fuel stream is assumed to be the main source of carbon precursor. This assumption is based on the widely held view that the hydrocarbon fuel itself is the main precursor for CNT growth alongside carbon monoxide [37,38]. Furthermore, sensitivity analysis showed that the use of other carbon precursors as carbon source did not result in better reproduction of the location of high yield region as observed in the experiment. The exclusion of carbon contribution from other intermediate species is deemed suitable in the present study considering the present objective to validate the growth region semi-qualitatively. The difficulties in the CNT growth rate measurement does not allow a fully quantitative validation of the predicted growth region.

2.2 Multi-scale Model

In the present study, a multi-scale modelling is employed to capture the reacting flow physics at the flame scale as well as the CNT growth processes at the particle scale. The CNT growth parameters in flames such as temperature and carbon precursor composition are resolved through CFD calculation. In the present study, a counter-flow flame model was constructed with the open-source

CFD toolkit OpenFOAM. A standard solver for non-premixed combustion of gaseous fuel that is incompressible and transient called reactingFoam is employed in the present study on laminar flame. The standard solver is able to model turbulent flow though the turbulence is not considered in the present study. An Euler implicit time integration method is employed along with the PIMPLE velocity-pressure coupling procedure.

The boundary conditions of the baseline model were determined based on previous experimental set-up that consists of two identical, vertically aligned, cylindrical burners with a separation distance of 22 mm [18]. The upper burner that introduces the fuel stream consists of methane, ethylene, and nitrogen with respective volume percentages of 25%, 5%, and 70%. The lower burner introduces the oxidizer with 21% of oxygen and 79% of nitrogen. In the experiment, the opposing flow of oxidizer and fuel at an exit velocity of 15cm/s generates a one-dimensional flame. Nickel catalyst is introduced in the form of a mesh confined in a circular holder of 3 mm diameter. The pure nickel mesh is constructed of 200 square grids and serves as both the catalyst and the CNT growth site. Considering the overall size of the catalyst mesh (3 mm) to be an order of magnitude smaller than the diameter of the burner (46 mm) [18], the mesh is assumed to have minimal effect on the flow field. Therefore, the mesh geometry is excluded in the present model to allow overall mapping of growth region within the flame. A 2-D domain is deemed sufficient to capture the flow field of the flame that stabilizes near the shear layer. The grid independence is achieved with 28,000 cells based on the temperature profile at the centreline. The flame solutions are then used as inputs for the CNT growth model at the particle scale.

A two-step reaction mechanism proposed by Westbrook and Dryer [35] was employed to model the chemical reaction of the reacting flow of methane-ethylene mixture. The use of detailed chemistry is deemed unnecessary at this stage due to the assumption of methane as the main carbon precursor for CNT growth as discussed at length in section 2.1. Table 1 shows the two-step reactions for CH_4 and C_2H_4 and their corresponding reaction rate parameters which describe the rate constant, $k = AT^n exp(E_a/RT)$ where A, T, n, E_a and R are pre-exponential factor, the gaseous temperature, the temperature exponent, the activation energy, and the universal gas constant respectively [35].

Table 1
List of reactions and their corresponding pre-exponential factors and activation energies for the two-step mechanism of the present study [35].

Reaction	A (s^{-1})	E_a (cal/mol)
$CH_4 + 2O_2 \rightarrow CO_2 + 2H_2O$	1.3×10^8	30000
$C_2H_4 + 3O_2 \rightarrow 2CO_2 + 2H_2O$	2.0×10^{12}	30000
$CO_2 \rightarrow CO + 0.5O_2$	5.0×10^8	40000
$CO + H_2O + 0.5O_2 \rightarrow CO_2 + H_2O$	3.98×10^{14}	40000

At the post-processing stage, the CNT length is mapped throughout the counterflow flame domain to determine the region of high yield. The effects of flame strain rate on CNT growth was then investigated and the respective CNT length was mapped and compared with the baseline case. The strain rate that varies with different inlet velocity, is given as $a = 2/L(U_a + U_f (\rho_a/\rho_f)^{1/2})$, where L, U_a, U_f, ρ_a and ρ_f are fixed burner distance of 22 mm, oxidizer inlet velocity, fuel inlet velocity, oxidizer density, and fuel density respectively. The CPU time taken for the post-processing computation is a few minutes whereas the CFD simulation took approximately an hour using a computer with Intel Core i7-5500u processor (4M Cache, 2.4GHz) where three processors are utilised in parallel.

3. Results and Discussion

3.1 Particle-Scale Model: Prediction of CNT Length

The particle-scale model that was recently developed for catalytic growth of CNTs [28] was validated against the measured CNT length in a CVD synthesis where acetylene was used as carbon source with cobalt as catalyst at a temperature and partial pressure of 1100 K and 20 Torr respectively [39]. At present, CNT length validation for flame synthesis is still a challenge due to the scarce data available in flame synthesis studies. Nonetheless, owing to the similarity of the basic chemical process that happens in CVD and flame synthesis, the present comparison with CVD is deemed reasonable though the residence time between the two synthesis methods are largely different. The validation that is illustrated in Figure 1 shows good agreement between the predicted and the measured CNT length where a rapid growth of the CNT length during the early period of the synthesis followed by a gradual increase of the length afterwards is reproduced. The present model predicts the length of CNT after the onset of steady growth period (after 100 s) accurately with a maximum error of 5%. Overall, the accuracy of the particle-scale model is satisfactory though a significant discrepancy between the predicted and measured growth rate is seen during the transient growth region due to the large measurement uncertainty at rapid growth rate.
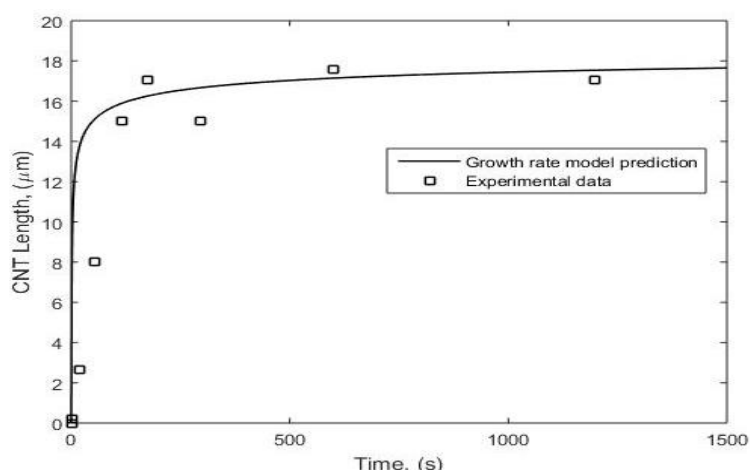

Fig. 1. Comparison between the predicted CNT length using the particle-scale model and the measured CNT length in CVD [39].

3.2 Multi-Scale Model: Prediction of CNT Growth Region Location

The 2-dimensional model used in the present study is validated by comparing the present result with the published experimental work [18] where the volume percentage of CH_4, C_2H_4, and N_2 are 25%, 5% and 70% respectively. The predicted temperature profile at the strain rate of 26 s^{-1} is plotted in Figure 2, which reproduces the trend of measured temperature where the temperature is increasing towards the flame front. In the experiment, the temperature measurements were taken at the centreline along vertical direction from approximately 11 mm to 17 mm height as evident from Figure 2. This region lies between the lower burner (oxidizer inlet) at 0 mm and the upper burner (fuel inlet) at 22 mm. The average error of 15% in the temperature prediction is considered acceptable given that the radiative heat loss is not included in the present modelling and experimental uncertainty that was not documented in the original publication [18]. Large fluctuation in the measured temperature could be due to the effect of flow disturbance caused by the

thermocouple tip, which is not modelled in the present study. However, the overall accuracy of the model in the prediction of temperature magnitude and distribution is deemed satisfactory. The deposition time of the CNTs growth was fixed at 120 s based on the exposure time in the experiment as reported previously [18].
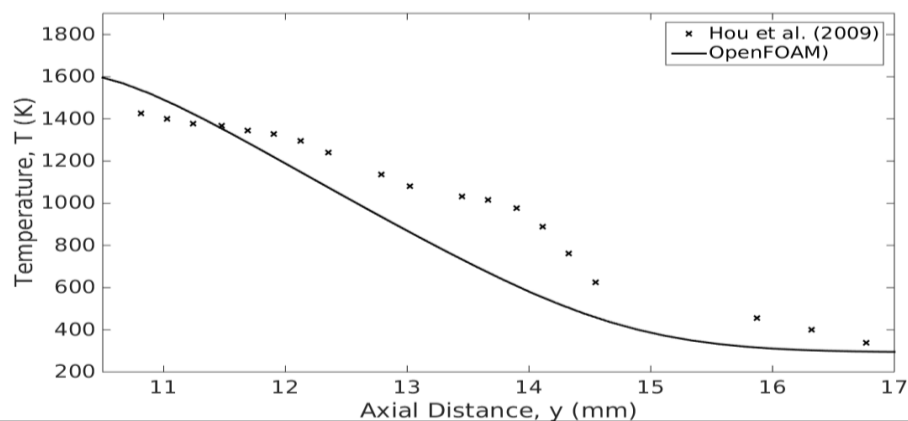

Fig. 2. Comparison between the predicted and the measured temperature [18] of the counter-flow diffusion flame along the center line of the fuel side.

Figures 3(a) and 3(b) illustrate the flame structure in the mixture fraction and physical space respectively overlapped with the predicted region of high yield. The mixture fraction is calculated based on Eq. (4) where v, Y_F, Y_{O2}, $Y_{F,1}$, and $Y_{O2,2}$ are stoichiometric mass ratio, fuel mass fraction, oxidiser mass fraction, fuel mass fraction in the fuel stream, and oxidiser mass fraction in the oxidiser stream respectively where $Z=1$ and $Z=0$ occur at the fuel and oxidiser inlets respectively. Stoichiometric mixture fraction Z_{st} = 0.22 for methane-ethylene-air flame that is calculated based on Eq. (5) is an indicator of flame location that corresponds to 10 mm downstream of the oxidiser inlet as shown in Figure 3(b).

$$Z = \frac{vY_F - Y_{O2} + Y_{O2,2}}{vY_{F,1} + Y_{O2,2}} \tag{4}$$

$$Z_{st} = \frac{Y_{O2,2}}{vY_{F,1} + Y_{O2,2}} \tag{5}$$

Figure 3(b) shows that the present study successfully predicts the high yield region in the rich side of the flame where the supplied heat is adequate enough to produce the growth at nominal methane concentration of 0.05. The flame location is slightly offset from the maximum temperature location as expected. A parabolic shape of temperature profile is predicted due to the heat transfer in both directions from the flame with all reactant concentrations reduce towards the flame front. The mass diffusion of products away from the reaction zone results in the parabolic shape of the product species.
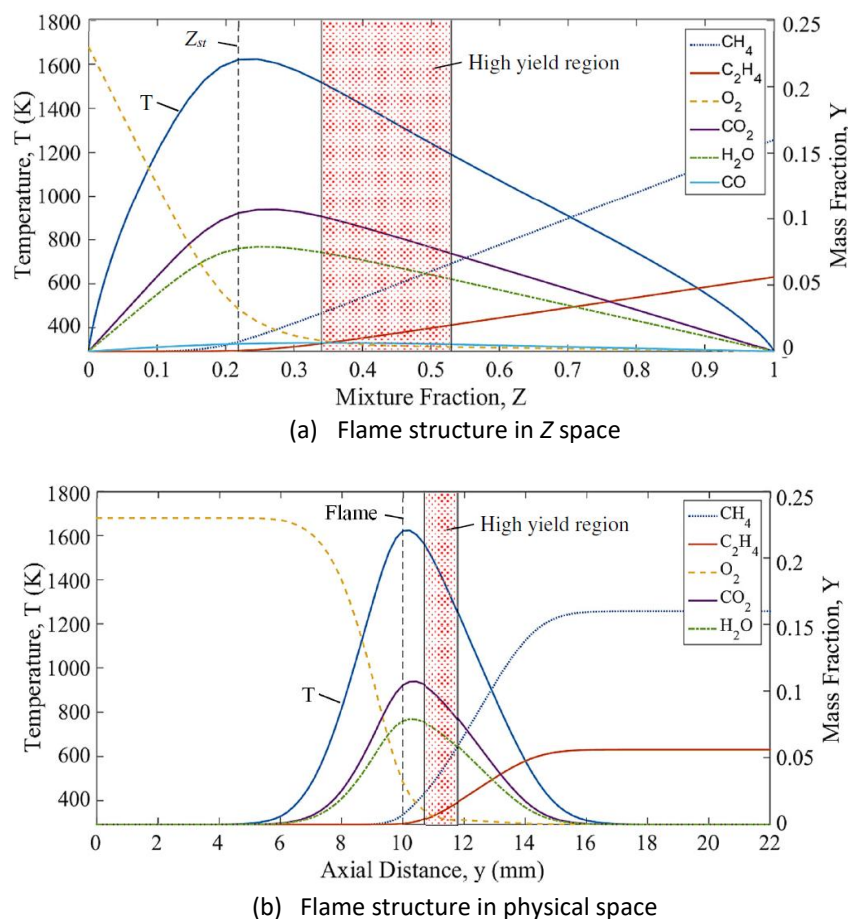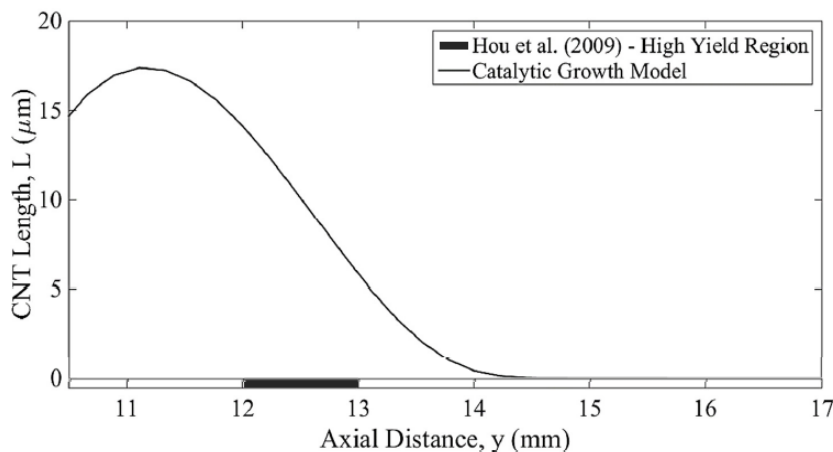
(a) Flame structure in *Z* space

(b) Flame structure in physical space

Fig. 3. Flame structure, reaction zone, and high yield region of the counter flow diffusion flame at 25 s^{-1} strain rate.
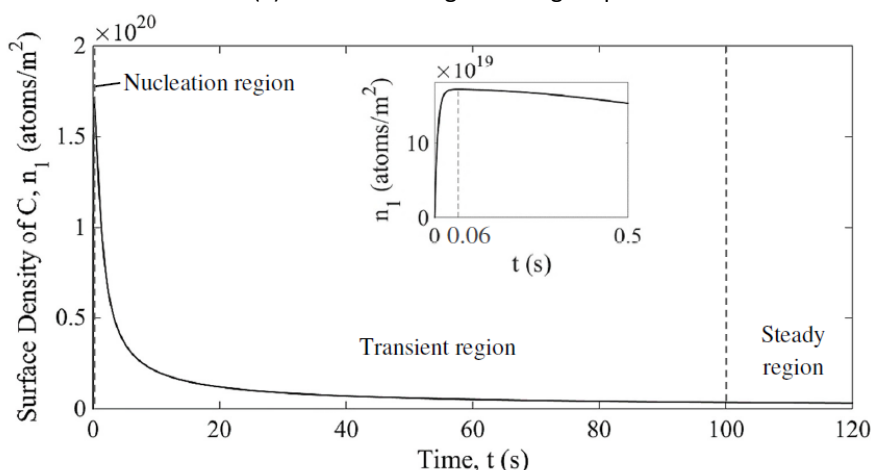
Referring to Figure 3(b), the high yield region is predicted in the range of 10.7 mm and 11.8 mm downstream of the oxidiser inlet that agrees quite well with respective experimental observation [18] that reported the range of high growth region that is between 12.1 mm and 13.0 mm respectively. The present study proposed a determination of high yield region based on the location of 10% length deviation from the maximum predicted length of CNT. The prediction of CNT length at varying axial location is shown in Figure 4(a) where the predicted high growth region corresponds to the 10% deviation from the maximum predicted CNT length of 15 µm. Similar technique of reporting CNT growth region has been employed by a recent modelling study that successfully validated CNT growth region at different flame heights in an inverse diffusion flame [40]. The experimental observation on the growth region that was done qualitatively based on SEM image of the synthesized CNT at the same operating condition [18] is indicated by the black bar at the bottom of Figure 4(a). The prediction of high yield region in the present study that is deviated by about 1 mm is considered acceptable realizing the inherent experimental uncertainty due to the qualitative approach of growth region determination. To the best of authors knowledge, the present study represents the first attempt to predict the high yield region of CNT growth in flame synthesis based on a semi-quantitative approach. The catalytic growth is governed by the temperature and the concentration of carbon precursors, where the growth generally increases with the increment of both factors.

Figure 4(b) illustrates the corresponding surface density of carbon atoms n_1 and its respective growth region over time. The catalytic growth regions are categorised into three regions that are nucleation, transient, and steady regions. In the nucleation region, the deposited carbon atoms accumulate on the catalyst particle surface and saturate at 0.06s, with a peak surface density n_1 of

1.7×10^{20} atoms/m^2, as shown in the inset. Nucleation region is the region with the highest growth rate of CNT that is followed by the transient region where carbon atoms rapidly diffuse into the catalyst particle. The CNT length gradually increased in the transient region. Finally, the steady region starts after the transient region at about 100s, where steady diffusion of carbon atoms into the catalyst particle happens. The reduction in diffusion rate is due to catalyst deactivation by inactive catalyst particles and encapsulation of amorphous carbon. A detailed validation of the particle-scale model is included elsewhere [28].

(a) Validation of growth region prediction

(b) The change of surface density of carbon atom with time.

Fig. 4. Prediction of CNT growth region using a multi-scale model.

3.3 Effects of Flame Strain On Growth Region

Referring to Figure 5 that shows the flame temperature, methane mass fraction, and CNT length, further reduction in temperature results in the same reduction of growth rate in the direction away from the flame front. Despite the increase in temperature towards the flame front at $y=10$ mm, the growth reduces due to the low concentration of carbon precursor that is almost consumed completely. Referring to Figure 3, the predicted temperature range for the high yield region is between 1300 K to 1600 K that falls within a reasonable range based on previous experimental observations on CNT catalytic growth [18,32,41,42]. The present observation on the temperature range of high yield region simply serves as a preliminary verification of the model since the range of

temperature for high yield region may change based on the inlet conditions of the burner or the catalyst parameters.

The strain rate effect was studied with the variation of strain rates from 26 s^{-1} to 150 s^{-1}. The strain rate effects on flame temperature, methane mass fraction, and CNT length is shown in Figure 5. The trend for temperature profile at increasing strain rate agrees with a previous experimental study [32] where a shift of maximum temperature location towards the fuel side is observed as strain rate increases. The extent of high temperature region reduces as the strain rate increases due to the increase in shear stress that results in the thinning of shear layer. Due to the increase in mass flow rate of the fuel, the mass fraction of methane within the high yield region increases at high strain rate. In addition, the growth region indicated by the CNT length distribution in Figure 5(b) follows a bell-shaped curve. Interestingly, the trend of growth rate and CNT length in the present flame configuration is dictated by the temperature profile and the high growth region is determined by the balance between temperature and mass fraction of carbon precursor.

A closer observation of Figure 5(b) reveals that the CNT length is slightly increased as the strain rate increases. This is due to the fact that more carbon source is available for adsorption, diffusion, and nucleation of CNT through a catalyst particle during the catalytic growth of CNT. The increment in methane mass fraction contributes to the adsorption term in the growth rate model where an increase in fuel mass fraction results in increased flux of carbon source molecules and hence the increased deposition rate of carbon source on catalyst particle.
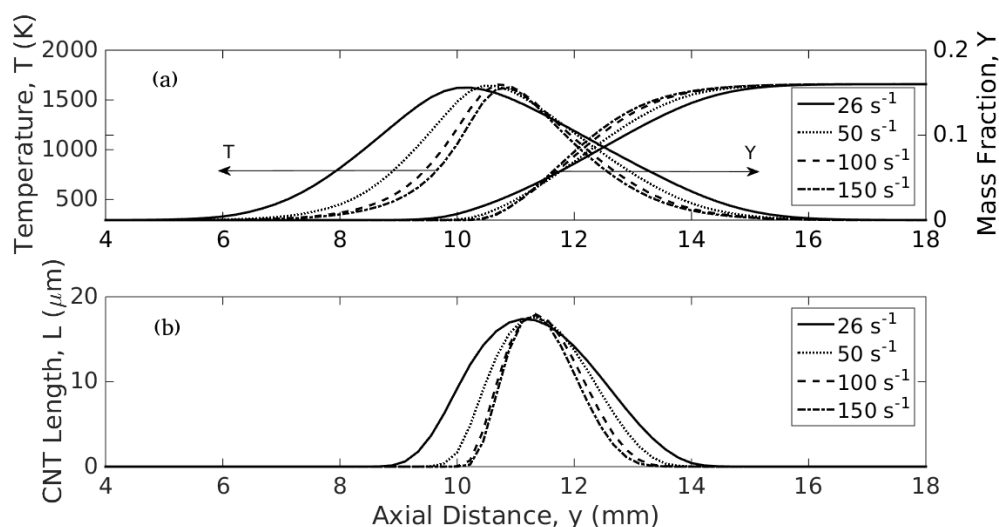

Fig. 5. Distribution of (a) temperature and methane mass fraction and (b) CNT length along the flame centerline.

Figure 6 illustrates the surface plot of CNT length within the flame and the temperature contour overlapped with the streamlines at strain rates of 26 s^{-1} and 150 s^{-1} respectively. The high temperature region is located at the shear layer of the fuel and the oxidizer streams. As the strain rate is increased, the shear layer becomes flatter due to the inertial effects on the flow field that becomes more dominant compared to the buoyancy effect. The overall distribution trend of growth region in Figure 6(a) and 6(c) that follows the temperature profiles in Figure 6(b) and 6(d) respectively verify the earlier observation on the effects of the flame structure on the growth rate distribution. Referring to Figures 6(a) and 6(c), the flame with low strain rate provides a parabolic and larger area of growth compared to that of high strain rate. On the other hand, the flat region of growth for flame with high flame strain suggests a more efficient CNT collection considering the conventional flat shape of catalyst substrate that is normally adopted in the large-scale synthesis. It could be inferred

from Figure 5(a) that there is a shift in maximum temperature location from 10 mm to 11 mm along the centreline that results in the respective shift in the growth region.
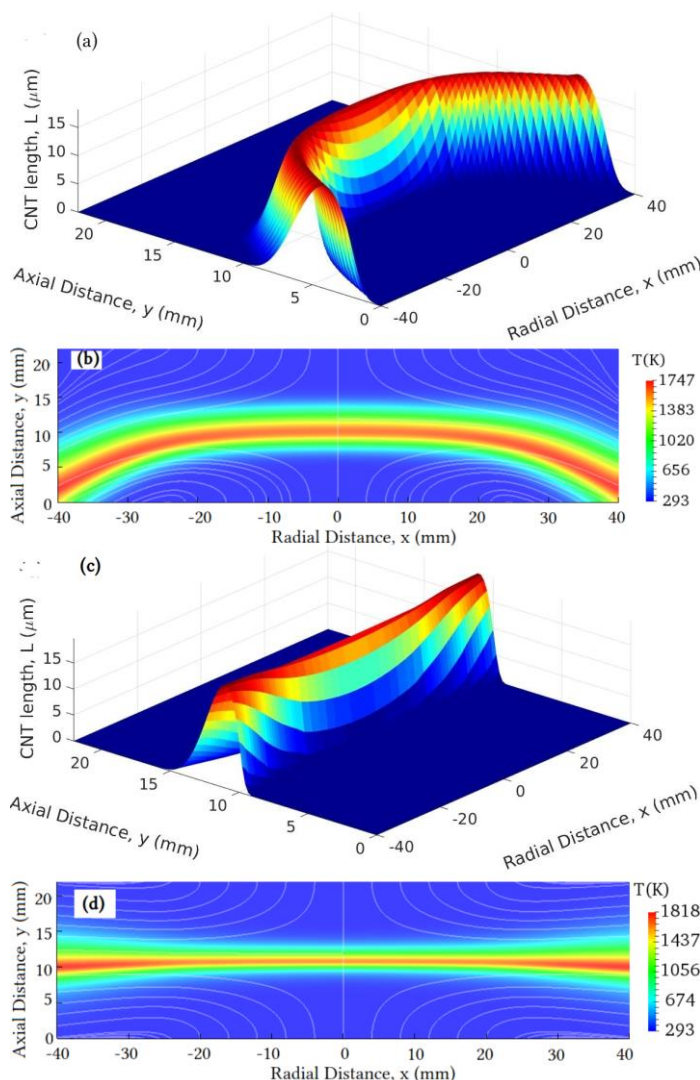

Fig. 6. Surface plot of predicted CNT length at strain rate of (a) 26 s^{-1} (c) 150 s^{-1}; and predicted temperature overlapped with the streamlines at strain rate of (b) 26 s^{-1} (d) 150 s^{-1}.

4. Conclusions

In the present study, a multi-scale model of flame synthesis is employed on a methane-ethylene diffusion flame with counter-flow burner configuration. A multi-scale modelling approach is adopted with an assumption that methane is the only carbon source for CNT growth to allow preliminary prediction of the growth region in the whole flame. Based on CNT length measurement at different synthesis period in a CVD experiment, a previously developed model for catalytic growth of CNT has successfully reproduced the change of CNT length over time. Predicted profile of axial temperature in laminar flame solution shows satisfactory agreement with the experiment based on the temperature magnitude along the centreline in the axial direction though the local temperature fluctuation failed to be reproduced. A multi-scale model that coupled the reacting flow solution at flame scale and that of the CNT length prediction at particle scale yields a semi-quantitative determination of the high yield region. Compared to the experimental observation, the predicted

location of high yield region is accurate within 1 mm. The present model successfully predicts the high yield region on the fuel side of the flame where the local mixture fraction is rich and the prediction of high growth region corresponds to the temperature range of 1200 K to 1500 K with the methane nominal mass fraction of 0.05. The opposing trend of temperature and methane concentration results in the reduction of growth rate on both sides of the high yield region. As flame strain rate increases, a flat flame is produced due to the dominance of the inertial effects over the buoyancy effects. The resulting flat high growth region at high flame strain rate favours efficient growth and collection of CNTs in large-scale setup where employment of flat substrate system is more common and convenient. On the other hand, the parabolic growth region from the flame with low strain rate provides larger high growth region though acquiring efficient CNT collection would become a challenge when entering scale-up production. The location of maximum growth is shifted towards the fuel side in response to the shift in maximum temperature location in the same direction. While the trend of CNT growth rate is governed by the temperature distribution, the location of high growth region is determined by optimum temperature and carbon precursor concentration.

Acknowledgement

References

[1]   De Volder, Michael F. L., Sameh H. Tawfick, Ray H. Baughman, and A. John Hart. "Carbon nanotubes: present and future commercial applications." *Science* 339, no. 6119 (2013): 535-539.
[2]   Jamil, Muhammad Mahmud, Nor Azwadi Che Sidik, Umar Sanusi Umar, Muhammad Tukur Hamisu, and Aisha Sa'ad. "Carbon nanotube for solar energy applications: A review." *Journal of Advanced Research in Fluid Mechanics and Thermal Sciences* 56, no. 2 (2019): 233-247.
[3]   Mohamad, Ahmad Tajuddin, Jesbains Kaur, Nor Azwadi Che Sidik, and Saidur Rahman. "Nanoparticles: A review on their synthesis, characterization and physiochemical properties for energy technology industry." *Journal of Advanced Research in Fluid Mechanics and Thermal Sciences* 46, no. 1 (2018): 1-10.
[3]   Zhang, Qiang, Jia-Qi Huang, Wei-Zhong Qian, Ying-Ying Zhang, and Fei Wei. "The road for nanomaterials industry: A review of carbon nanotube production, post-treatment, and bulk applications for composites and energy storage." *Small* 9, no. 8 (2013): 1237-1265.
[5]   Wu, Jianpeng, Kaiheng Liang, Chaoqiang Yang, Jie Zhu, and Dong Liu. "Synthesis of carbon nanotubes on metal mesh in inverse diffusion biofuel flames." *Fullerenes, Nanotubes and Carbon Nanostructures* 27, no. 1 (2019): 77-86.
[6]   Merchan-Merchan, Wilson, Alexei V. Saveliev, Lawrence Kennedy, and Walmy Cuello Jimenez. "Combustion synthesis of carbon nanotubes and related nanostructures." *Progress in Energy and Combustion Science* 36, no. 6 (2010): 696-727.
[7]   Zainal, Muhammad Thalhah, Mohd Fairus Mohd Yasin, and Mazlan Abdul Wahid. "Optimizing flame synthesis of carbon nanotubes: experimental and modelling perspectives." *Jurnal Teknologi* 78, no. 8-4 (2016).
[8]   Hamzah, N., M.F Mohd Yasin, M.Z. Mohd Yusop, A. Saat, and N.A. Mohd Subha. "Rapid production of carbon nanotubes: a review on advancement in growth control and morphology manipulations of flame synthesis." *Journal of Materials Chemistry A* 5, no. 48 (2017): 25144-25170.
[9]   Richter, Henning, Meri Treska, Jack B. Howard, John Z. Wen, Sebastien B. Thomasson, Arthur A. Reading, Paula M. Jardim, and John B. Vander Sande. "Large scale combustion synthesis of single-walled carbon nanotubes and their characterization." *Journal of nanoscience and nanotechnology* 8, no. 11 (2008): 6065-6074.
[10]   Mittal, Garima, Vivek Dhand, Kyong Yop Rhee, Hyeon-Ju Kim, and Dong Ho Jung. "Carbon nanotubes synthesis using diffusion and premixed flame methods: a review." *Carbon letters* 16, no. 1 (2015): 1-10.
[11]   Jourdain, Vincent, and Christophe Bichara. "Current understanding of the growth of carbon nanotubes in catalytic chemical vapour deposition." *Carbon* 58 (2013): 2-39.
[12]   Camacho, Jorge, and Ahsan R. Choudhuri. "Effects of fuel compositions on the structure and yield of flame synthesized carbon nanotubes." *Fullerenes, Nanotubes, and Carbon Nanostructures* 15, no. 2 (2007): 99-111.

[13] Choudhuri, Ahsan, Jorge Camacho, and Jack Chessa. "Flame synthesis of coiled carbon nanotubes." *Fullerenes, Nanotubes, and Carbon Nonstructures* 14, no. 1 (2006): 93-100.

[14] Hall, Brendan, Chuanwei Zhuo, Yiannis A. Levendis, and Henning Richter. "Influence of the fuel structure on the flame synthesis of carbon nanomaterials." *Carbon* 49, no. 11 (2011): 3412-3423.

[15] Unrau, Chad J., Richard L. Axelbaum, and Phil Fraundorf. "Single-walled carbon nanotube formation on iron oxide catalysts in diffusion flames." *Journal of Nanoparticle Research* 12, no. 6 (2010): 2125-2133.

[16] Chung, De-Hua, and Ta-Hui Lin. "Nitrogen dilution effect on flame synthesis of carbon nanostructures with acoustic modulation." *The Journal of Physical Chemistry C* 115, no. 33 (2011): 16287-16294.

[17] Manciu, Felicia S., Jorge Camacho, and Ahsan R. Choudhuri. "Flame Synthesis of Multi-walled Carbon Nanotubes Using CH4-H2 Fuel Blends." *Fullerenes, Nanotubes and Carbon Nanostructures* 16, no. 4 (2008): 231-246.

[18] Hou, Shuhn-Shyurng, De-Hua Chung, and Ta-Hui Lin. "High-yield synthesis of carbon nano-onions in counterflow diffusion flames." *Carbon* 47, no. 4 (2009): 938-947.

[19] Hamzah, Norikhwan, Mohd Fairus Mohd Yasin, Mohd Zamri Mohd Yusop, Muhammad Thalhah Zainal, and Muhammad Arif Fikri Rosli, "Identification of CNT growth region and optimum time for catalyst oxidation: Experimental and modelling studies." *Evergreen Joint Journal of Novel Carbon Resource Sciences & Green Asia Strategy* 6, no. 1 (2019): 85-91.

[20] Hou, Shuhn-Shyurng, Wei-Cheng Huang, and Ta-Hui Lin. "Flame synthesis of carbon nanostructures using mixed fuel in oxygen-enriched environment." *Journal of Nanoparticle Research* 14, no. 11 (2012): 1243.

[21] Hu, Wei-Chieh, and Ta-Hui Lin. "Ethanol flame synthesis of carbon nanotubes in deficient oxygen environments." *Nanotechnology* 27, no. 16 (2016): 165602.

[22] Li, Q. W., Yuan Li, X. F. Zhang, Satishkumar B. Chikkannanavar, Y. H. Zhao, Andrea M. Dangelewicz, L. X. Zheng et al. "Structure-dependent electrical properties of carbon nanotube fibers." *Advanced Materials* 19, no. 20 (2007): 3358-3363.

[23] Naha, Sayangdev, Swarnendu Sen, Anindya K. De, and Ishwar K. Puri. "A detailed model for the flame synthesis of carbon nanotubes and nanofibers." *Proceedings of the combustion institute* 31, no. 2 (2007): 1821-1829.

[24] Wen, John Z., Matthew Celnik, Henning Richter, Meri Treska, John B. Vander Sande, and Markus Kraft. "Modelling study of single walled carbon nanotube formation in a premixed flame." *Journal of Materials Chemistry* 18, no. 13 (2008): 1582-1591.

[25] Endo, Hajime, Kazunori Kuwana, Kozo Saito, Dali Qian, Rodney Andrews, and Eric A. Grulke. "CFD prediction of carbon nanotube production rate in a CVD reactor." *Chemical Physics Letters* 387, no. 4-6 (2004): 307-311.

[26] Kuwana, Kazunori, and Kozo Saito. "Modeling CVD synthesis of carbon nanotubes: Nanoparticle formation from ferrocene." *Carbon* 43, no. 10 (2005): 2088-2095.

[27] Naha, Sayangdev, and Ishwar K. Puri. "A model for catalytic growth of carbon nanotubes." *Journal of Physics D: Applied Physics* 41, no. 6 (2008): 065304.

[28] Zainal, M. T., Mohd Fairus Mohd Yasin, and Mazlan Abdul Wahid. "Investigation of the coupled effects of temperature and partial pressure on catalytic growth of carbon nanotubes using a modified growth rate model." *Materials Research Express* 3, no. 10 (2016): 105040.

[29] Zainal, M.T. Mohd Fairus Mohd Yasin, Muhammad Abid Ira Irawan, Muhammad Faizullizam Roslan, Norikhwan Hamzah, and Mohd Zamri Mohd Yusop. "Investigation on the deactivation of cobalt and iron catalysts in catalytic growth of carbon nanotube using a growth rate model." *Journal of Advanced Research in Materials Science* 51, no. 1 (2018): 11-22.

[30] Memon, Nasir K., Fusheng Xu, Geliang Sun, Sage JB Dunham, Bernard H. Kear, and D. Tse Stephen. "Flame synthesis of carbon nanotubes and few-layer graphene on metal-oxide spinel powders." *Carbon* 63 (2013): 478-486.

[31] Pitz, Robert W., Shengteng Hu, Pieyong Wang, "Tubular premixed and diffusion flames: effect of stretch and curvature." *Progress in Energy and Combustion Science* 42 (2014):1-34.

[32] Li, T. X., H. G. Zhang, F. J. Wang, Z. Chen, and K. Saito. "Synthesis of carbon nanotubes on Ni-alloy and Si-substrates using counterflow methane–air diffusion flames." *Proceedings of the Combustion Institute* 31, no. 2 (2007): 1849-1856.

[33] Woo, S.K., Y.T. Hong, O.C. Kwon, "Flame-synthesis limits and self-catalytic behaviour of carbon nanotubes using a double-faced wall stagnation flow burner." *Combustion and Flame* 156, no. 10 (2009): 1983-1992.s

[34] Hou, Shuhn-Shyurng, and Wei-Cheng Huang. "Influence of oxygen concentration, fuel composition, and strain rate on synthesis of carbon nanomaterials." *Journal of nanoparticle research* 17, no. 2 (2015): 65.

[35] Westbrook, Charles K., and Frederick L. Dryer. "Chemical kinetic modeling of hydrocarbon combustion." *Progress in Energy and Combustion Science* 10, no. 1 (1984): 1-57.

[36] Puretzky, Alexander A., David B. Geohegan, Stephen Jesse, Ilia N. Ivanov, and Gyula Eres. "In situ measurements and modeling of carbon nanotube array growth kinetics during chemical vapor deposition." *Applied Physics A* 81, no. 2 (2005): 223-240.

[37] Chong, Cheng Tung, Win Hon Tan, Siew Ling Lee, William Woei Fong Chong, Su Shiung Lam, and Agustin Valera-Medina. "Morphology and growth of carbon nanotubes catalytically synthesised by premixed hydrocarbon-rich flames." *Materials Chemistry and Physics* 197 (2017): 246-255.

[38] Suzuki, S., and S. Mori. "Considerations on the key precursor for the growth of carbon nanotubes using a diesel engine as a reactor." *Chemical Engineering Science* 186 (2018): 62-73.

[39] Bower, Chris, Otto Zhou, Wei Zhu, D. J. Werder, and Sungho Jin. "Nucleation and growth of carbon nanotubes by microwave plasma chemical vapor deposition." *Applied Physics Letters* 77, no. 17 (2000): 2767-2769.

[40] Zainal, Muhammad Thalhah. "Modelling the flame synthesis of carbon nanotube (cnt) in inverse diffusion flame." Master thesis, Universiti Teknologi Malaysia, 2017.

[41] Yuan, Liming, Kozo Saito, Wenchong Hu, and Zhi Chen. "Ethylene flame synthesis of well-aligned multi-walled carbon nanotubes." *Chemical physics letters* 346, no. 1-2 (2001): 23-28.

[42] Lee, Gyo Woo, Jongsoo Jurng, and Jungho Hwang. "Synthesis of carbon nanotubes on a catalytic metal substrate by using an ethylene inverse diffusion flame." *Carbon* 42, no. 3 (2004): 682-685.